IET Circuits, Devices & Systems

Research Article

IET Journals
The Institution of Engineering and Technology

Compact noise modelling for common double-gate metal–oxide–semiconductor field-effect transistor adapted to gate-oxide-thickness asymmetry

ISSN 1751-858X
Received on 4th February 2015
Accepted on 12th July 2015
doi: 10.1049/iet-cds.2015.0128
www.ietdl.org

Neha Sharan ✉, *Santanu Mahapatra*

Nano Scale Device Research Laboratory, Department of Electronic Systems Engineering, Indian Institute of Science, Bangalore 560012, India

✉ *E-mail: nehasharan11@yahoo.com*

Abstract: On the basis of the quasi-linear relationship between the surface potentials of a common double-gate metal–oxide–semiconductor field-effect transistor, a compact noise model, which is adapted to gate-oxide-thickness asymmetry, is proposed. The proposed model includes a physics-based thermal and flicker noise model. The effect of the lateral and vertical electric fields on the mobility degradation has also been taken into account for accurate noise prediction in short-channel devices. The thermal noise model is compared with the technology computer aided design (TCAD) simulation data and good agreement is observed. The proposed noise model appears to be efficient for analogue circuit simulation.

1 Introduction

Common double-gate metal–oxide–semiconductor field-effect transistor (CDG-MOSFET) has emerged as one of the most viable option to replace the bulk MOSFET in sub-32 nm technology nodes [1, 2] due to its improved electrostatic integrity and better gate control over the channel. For successful utilisation of these devices in radio frequency (RF) analog circuit applications efficient compact noise models are required to predict the noise characteristics accurately at both the low- and high-frequency domain. Noise at low frequency is dominated by the flicker noise ($1/f$) and at high frequency by the thermal noise. Although flicker noise is predominant only at low frequency, in some circuits such as voltage controlled oscillator, where upconversion is performed, it has an impact also on the high-frequency device behaviour. There are two distinct models to describe the origin of flicker noise: carrier number fluctuation and mobility fluctuation [3, 4]. Carrier number fluctuation in the channel as proposed by McWorther [5] is due to the random trapping and de-trapping of charge carriers in the oxide traps at the Si–SiO_2 interface. Mobility fluctuation as proposed by Hooge law [6] is attributed to the phonon scattering. It is observed that at bias conditions below the threshold voltage, flicker noise is dominated by the mobility fluctuation and above threshold it is dominated by carrier number fluctuation [7]. Thus, in this work, we propose a unified flicker noise model based on both these phenomenon. Thermal noise on other hand is generated due to random Brownian motion of electrons which leads to heating of the charge carriers in channel. Thermal noise is best described by Klaassen–Prins equation [3] and therefore, in this paper, we have used this equation to model thermal noise. Moreover, in order to make the model suitable for submicron devices, it is important to consider the field-dependent electron mobility degradation on noise performance [8, 9]. We have incorporated the effect of lateral and perpendicular electric field through mobility and conductance expression. The proposed noise model is based on our recent work on small-channel length CDG-MOSFET [10] and found to be working efficiently in all operating regimes. Due to the lack of experimental results thermal noise model has been verified against TCAD [11] simulation results. Since TCAD does not provide flicker noise simulation model, we cannot validate the proposed flicker noise model. However, it is observed that the characteristics and the range of flicker noise predicted from the model matches closely with experimental results for the symmetric devices.

2 Model development

The conventions used in this paper are: $t_{ox_1}(2)$ is the oxide thickness of first(second) gate, t_{si} is the thickness of the silicon body, $C_{ox_1}(2)$ is the oxide capacitance per unit area of first (second) gate defined as $\varepsilon_{ox}/t_{ox_1}(2)$, ε_{si}, ε_{ox} are the permittivities of Si and SiO_2, respectively, q is the elementary charge, β is the inverse thermal voltage, n_i is the intrinsic carrier density, $B = 2qn_i/\beta\varepsilon_{si}$, L is the channel length, W is the channel width, $\psi_{1(2)}$ is the Si/SiO_2 surface potentials at first (second) gate, V is the electron quasi-Fermi potential (channel potential) and μ is the low-field electron mobility. The effective gate voltage is defined as $V_{gs_1(2)} = V_{gs_1(2)_{applied}} - \delta\phi_{1(2)}$, where $V_{gs_1(2)_{applied}}$ is the voltage applied at gate terminals and $\delta\phi_{1(2)}$ is the work function difference of the gate material. The inversion charge density at any point along the channel is denoted by Q_i, which is the sum of two components Q_{i_1} and Q_{i_2} expressed as $Q_{i_1}(2) = C_{ox_1}(2)(V_{gs_1}(2) - \psi_{1(2)})$. In the following discussions, any variable with subscript 's' refers to its value at source end and 'd' refers to its value at drain end. The variable x denotes the direction along the thickness of the channel with $x = \pm t_{si}/2$ represent the front and back Si/SiO_2 interface. The variable y represents the direction along the length of the channel while $y = 0$ and L represents the source end and the drain end of the channel, respectively.

Existing compact models for CDG-MOSFETs [12–15] are based on the fundamental assumption of having symmetric gate-oxide thickness, as it greatly simplifies the model development process. Recently, we have demonstrated that the models could be generalised by considering the asymmetry between gate-oxide thickness as there could be a possibility of having asymmetry between the gate-oxide thickness due to process variations and uncertainties [10]. In that work, we however considered the mobility degradation in short-channel MOSFETs only due to the lateral electric field. To include the vertical field effect, in this work we use the following expressions [16]

$$\mu_{eff} = \mu \cdot \mu_{pa} \cdot \mu_{pe} \tag{1}$$

where

$$\mu_{\text{pa}} = \frac{1}{\left[1 + (\mu/v_{\text{sat}})(\text{d}V/\text{d}y)^2\right]^{1/2}} \tag{2}$$

$$\mu_{\text{pe}} = \frac{1}{\left[1 + (\mu/E_{\text{f}})(\text{d}V/\text{d}x)\right]^{1/2}} \tag{3}$$

Evaluating (1) and (3) gives

$$\mu_{\text{eff}} = \mu \cdot \mu_{\text{pa}} \cdot \frac{\mu_{\text{pe}_1} + \mu_{\text{pe}_2}}{\text{av}} \tag{4}$$

where av and E_{f} are model parameters, and mu_{pe_1} and mu_{pe_2} are obtained by evaluating (3) across the front and back surfaces as

$$\mu_{\text{pe}_1} = \frac{1}{\left[1 + (\mu/E_{\text{f}})(V_{\text{sat}_1}/t_{\text{ox}_1})\right]^{1/2}},$$

$$\mu_{\text{pe}_2} = \frac{1}{\left[1 + (\mu/E_{\text{f}})(V_{\text{sat}_2}/t_{\text{ox}_2})\right]^{1/2}}$$

here $V_{\text{sat1(2)}}$ is the respective saturation voltage across front and back surfaces, expression of which are given in (Fig. 1). Fig. 1 validates that the accuracy of improved model with incorporation of vertical field effect dependency.

The channel noise comprises of thermal noise and flicker noise. For modelling noise in CDG-MOSFET we first calculate the respective spectral density.

2.1 Thermal noise

As proposed in [17] the conventional Klaassen–Prin equation does not accurately account for the impact of velocity saturation and hence an improved Klaassen–Prin equation was suggested which works correctly in the presence of the velocity saturation. The drain current spectral density following this improved Klaassen–Prins equation is given by [17]

$$S_{\text{id}} = \frac{4\,kT}{I_{\text{ds}}L_{\text{e}}^2}\int_{V_{\text{s}}}^{V_{\text{d}}} g_{\text{o}}^2(V)\left[1 + \left(\frac{\mu}{v_{\text{sat}}}\frac{\text{d}V}{\text{d}y}\right)^2\right]\text{d}V \tag{5}$$

$$L_{\text{e}} = \frac{L\int_{V_{\text{s}}}^{V_{\text{d}}} g_{\text{c}}(V)\text{d}V}{\int_{V_{\text{s}}}^{V_{\text{d}}} g(V)\text{d}V} g_{\text{c}}$$

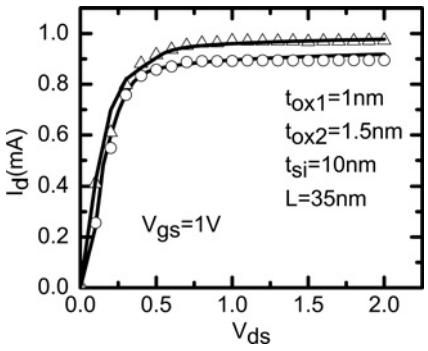

Fig. 1 *Drain current plot with variation in drain voltage as predicted by TCAD simulation (symbol) and proposed model (line). The triangle denotes characteristics including only mobility degradation due to lateral electric field (both in TCAD and model). The circle denotes characteristic, including mobility dependence on both lateral and vertical fields*

is the modified channel length and

$$g_{\text{c}}(V) = g(V)\left[\frac{g_{\text{o}}(V)}{g(V)}\right]^2$$

is the modified channel conductance The local conductance $g(V)$ with incorporation of velocity saturation could be expressed as

$$g(V) = g_{\text{o}}(V)\left[1 + \left(\frac{\mu}{v_{\text{sat}}}\frac{\text{d}V}{\text{d}y}\right)^2\right]^{1/2}$$

with $g_{\text{o}}(V) = \mu.\mu_{\text{pe}}WQ_{\text{i}}$.

Solving (5) results in an equation in terms of inversion charge across the channel and since in asymmetric CDG-MOSFET we have two surfaces with different potentials solving (5) directly is not trivial. Therefore, as proposed in [18], we linearise the potential across one surface in terms of the other to obtain the total inversion charge as

$$Q_{\text{i}} = Q_{i_1} + m_1 Q_{i_1} + c_1 \tag{6}$$

which yields

$$\frac{\text{d}V}{\text{d}Q_{i_1}} = -\frac{1}{C_{\text{ox}_1}} - \frac{\left(2nQ_{i_1} + p_1\right)}{\beta(nQ_{i_1}^2 + p_1Q_{i_1} + q_1)} \tag{7}$$

$$\frac{\text{d}Q_{i_1}}{\text{d}y} = \frac{1}{2\alpha_1 LQ_{i_1} + \gamma_1} \tag{8}$$

Here n, p_1, q_1, α_1 and γ_1 are the linearisation coefficients, expression of which could be found in [10, 18]. Finally on evaluating (5) using the above linearisation coefficients, we obtain

$$S_{\text{id}} = \text{CC}\int_{V_{\text{s}}}^{V_{\text{d}}} Q_{\text{i}}^2 \left[1 + \left\{\frac{\left(-1/C_{\text{ox}_1} - (2nQ_{i_1} + p_1)\beta^{-1}/(nQ_{i_1}^2 + p_1Q_{i_1} + q_1)\right)}{E_{\text{sat}}(2\alpha_1 Q_{i_1}L + \gamma_1 L)}\right\}^2\right]\text{d}V \tag{9}$$

where $\text{CC} = 4\,kT(\mu \cdot \mu_{\text{pe}}W)^2/I_{\text{ds}}L_{\text{e}}^2$ and $E_{\text{sat}} = v_{\text{sat}}/\mu$. Direct solution of (9) is not possible and therefore, based on the observation made through TCAD simulations, we approximate

$$-\frac{1}{C_{\text{ox}_1}} - \frac{1}{\beta}\frac{(2nQ_{i_1} + p_1)}{(nQ_{i_1}^2 + p_1Q_{i_1} + q_1)} \simeq f(Q_{i_1}) \tag{10}$$

where $f(Q_{i_1}) = A_{11}Q_{i_1} + B_{11}$ with $A_{11} = \dfrac{f(Q_{i_{1s}}) - f(Q_{i_{11d}})}{Q_{i_{1s}} - Q_{i_{11d}}}$, $B_{11} = \dfrac{f(Q_{i_{11d}})Q_{i_{1s}} - f(Q_{i_{1s}})Q_{i_{11d}}}{Q_{i_{1s}} - Q_{i_{11d}}}$, $Q_{i_{11d}} = m_q(Q_{i_{1s}} + Q_{i_{1d}})$, and m_q is the model parameter. Using this approximation we obtain

$$S_{\text{id}} = \text{CC}\int_{Q_{i_{1s}}}^{Q_{i_{1d}}} Q_{\text{i}}.f(Q_{i_1})\left[1 + \left\{\frac{\left(A_{11}Q_{i_1} + B_{11}\right)}{E_{\text{sat}}(2\alpha_1 Q_{i_1}L + \gamma_1 L)}\right\}^2\right]\text{d}Q_{i_1} \tag{11}$$

Evaluating which results in

$$I1_1=\frac{p_1\mathrm{CC}}{n}\left(\frac{\delta_1}{\beta C_{\mathrm{ox}_1}n}-\frac{p_1(nm_1^2+2nm_1+n)}{C_{\mathrm{ox}_1}n^2}\right) \tag{12}$$

$$I1_2=\mathrm{CC}\left(\frac{\beta q_1M_1^2+C_{\mathrm{ox}_1}p_1M_1^2+\beta c_1\delta_2+4c_1C_{\mathrm{ox}_1}nM_1}{\beta C_{\mathrm{ox}_1}n}\right) \tag{13}$$

$$I1_3=\frac{\mathrm{CC}q_1(\beta nm_1^2+2\beta nm_1+\beta n)}{\beta C_{\mathrm{ox}_1}n^2} \tag{14}$$

$$I1_4=\mathrm{CC}Q_{i_1}^2\left(\frac{\delta}{2\beta C_{\mathrm{ox}_1}n}+\frac{p_1(\beta nm_1^2+2\beta nm_1+\beta n)}{2\beta C_{\mathrm{ox}_1}n^2}\right) \tag{15}$$

$$I1_5=\frac{\mathrm{CC}\cdot\log(\Upsilon_1)\{p_1\vartheta_1-2nq_1M_1^2+c_1n\vartheta_2\}}{2\beta n^2} \tag{16}$$

$$I1_6=\frac{\mathrm{CC}\cdot\log(\Upsilon_2)(\vartheta_3-2c_1n(c_1n-\zeta-m_1\zeta)+2nq_1M_1^2}{2\beta n^2} \tag{17}$$

$$I1_7=\frac{\mathrm{CC}Q_{i_1}^3(\beta nm_1^2+2\beta nm_1+\beta n)}{3\beta C_{\mathrm{ox}_1}n} \tag{18}$$

$$I1=Q_{i_1}(I1_1-I1_2+I1_3)+I1_4-I1_5+I1_6 \tag{19}$$

where

$$\begin{aligned}\delta_1=&C_{\mathrm{ox}_1}(2n+2m_1^2n+4m_1n)\\&+\beta(p_1+m_1^2p_1+2c_1n+2m_1p_1+2c_1m_1n),\\ \delta_2=&c_1n+2p_1+2m_1p_1,\quad M_1=1+m_1,\end{aligned}$$

$$\Upsilon_1=p_1\zeta+\zeta^2+2Q_{i_1}n\zeta$$

$$\Upsilon_2=p_1\zeta-\zeta^2+2Q_{i_1}n\zeta$$

$$\zeta=\sqrt{p_1^2-4nq_1}$$

$$\vartheta_1=p_1+m_1^2p_1+2m_1p_1+\zeta+2m_1\zeta+m_1^2\zeta-2c_1m_1n-2c_1n$$

$$\vartheta_2=2c_1n-2\zeta-2m_1\zeta$$

$$\begin{aligned}\vartheta_3=&-p_1^2-m_1^2p_1^2-2m_1p_1^2+2m_1p_1\zeta+p_1\zeta+m_1^2p_1\zeta+2c_1m_1np_1\\&+2c_1np_1\end{aligned}$$

$$I2_1=\frac{\gamma_1\mathrm{CC}\mu^2A_{11}^2}{\alpha_1}\left(\frac{\varrho_1}{4L_\mathrm{e}^2\alpha_1^2v_{\mathrm{sat}}^2}-\frac{\gamma_1(A_{11}(1+m_1)^2)}{4L_\mathrm{e}^2\alpha_1^3v_{\mathrm{sat}}^2}\right) \tag{20}$$

$$I2_2=\frac{\mathrm{CC}(A_{11}^3c_1^2\mu^2+3A_{11}B_{11}c_1\mu^2\varrho_2)}{4L_\mathrm{e}^2\alpha_1^2v_{\mathrm{sat}}^2} \tag{21}$$

$$I2_3=\frac{\mathrm{CC}\gamma_1^2A_{11}^3\mu^2(1+m_1)^2}{16L_\mathrm{e}^2\alpha_1^4v_{\mathrm{sat}}^2} \tag{22}$$

$$I2_4=\frac{\mathrm{CC}(2c_1A_{11}^3\mu^2(1+m_1)+3B_{11}A_{11}^2\mu^2(1+m_1)^2)}{4L_\mathrm{e}^2\alpha_1^2v_{\mathrm{sat}}^2} \tag{23}$$

$$I2_5=\frac{\gamma_1\mathrm{CC}A_{11}^3\mu^2(1+m_1)^2}{4L_\mathrm{e}^2\alpha_1^3v_{\mathrm{sat}}^2} \tag{24}$$

$$I2_6=\frac{\mathrm{CC}A_{11}B_{11}c_1\mu^2\varrho_3}{4L_\mathrm{e}^2\alpha_1^2v_{\mathrm{sat}}^2} \tag{25}$$

$$I2_7=\frac{\mathrm{CC}(A_{11}^3c_1^2\mu^2+3A_{11}B_{11}\mu^2\varrho_4)}{8L_\mathrm{e}^2\alpha_1^2v_{\mathrm{sat}}^2} \tag{26}$$

$$I2_8=\mathrm{CC}4A_{11}^3c_1\alpha_1\gamma_1^3\mu^2\left(\alpha_1^2c_1+\gamma_1(1+m_1)\right) \tag{27}$$

$$I2_9=\mathrm{CC}A_{11}^3\gamma_1^5\mu^2(1+m_1)^2-24CCA_{11}^2B_{11}\alpha_1^3c_1^2\gamma_1^2\mu^2 \tag{28}$$

$$I2_{10}=6\mathrm{CC}A_{11}^2B_{11}\mu^2(1+m_1)^2\left(\frac{4\alpha_1^2c_1\gamma_1^3}{(1+m_1)}-6\alpha_1\gamma_1^4\right) \tag{29}$$

$$I2_{11}=48\mathrm{CC}A_{11}B_{11}^2\alpha_1^3c_1\gamma_1\mu^2(\alpha_1c_1-\gamma_1(1+m_1)) \tag{30}$$

$$I2_{12}=12\mathrm{CC}A_{11}B_{11}^2\alpha_1^2\gamma_1^3\mu^2(1+m_1)^2-32\mathrm{CC}B_{11}^3\alpha_1^5c_1^2\mu^2 \tag{31}$$

$$I2_{13}=8\mathrm{CC}B_{11}^3(4\alpha_1^4c_1\gamma_1\mu^2(1+m_1)-\alpha_1^3\gamma_1^2\mu^2(1+m_1)^2) \tag{32}$$

$$I2_{14}=\frac{CCA_{11}^3\mu^2(1+m_1)^2}{16L_\mathrm{e}^2\alpha_1^2v_{\mathrm{sat}}^2} \tag{33}$$

$$I2_{15}=12\mathrm{CC}A_{11}^3\alpha_1^2c_1^2\gamma_1^2\mu^2-16\mathrm{CC}A_{11}^3\alpha_1c_1\gamma_1^3\mu^2(1+m_1) \tag{34}$$

$$I2_{16}=5\mathrm{CC}A_{11}^3\gamma_1^4\mu^2(1+m_1)^2-48\mathrm{CC}A_{11}^2B_{11}\alpha_{11}^3c_1^2\gamma_1\mu^2 \tag{35}$$

$$I2_{17}=24\mathrm{CC}A_{11}^2\mu^2(1+m_1)^2\left(\frac{3\alpha_1^2c_1\gamma_1^2}{(1+m_1)}-B_{11}\alpha_1\gamma_1^3\right) \tag{36}$$

$$I2_{18}=48\mathrm{CC}A_{11}B_{11}^2\mu^2(\alpha_1^4c_1^2-2\alpha_1^3c_1\gamma_1(1+m_1)) \tag{37}$$

$$I2_{19}=36\mathrm{CC}A_{11}B_{11}^2\alpha_1^2\gamma_1^2\mu^2(1+m_1)^2 \tag{38}$$

$$I2_{20}=16\mathrm{CC}B_{11}^3(2\alpha_1^4c_1\mu^2(1+m_1)-\alpha_1^3\gamma_1\mu^2(1+m_1)^2) \tag{39}$$

$$\begin{aligned}I2=&Q_{i_1}\left\{\frac{\gamma_1(I2_1-I2_2+I2_3)}{\alpha_1}-\frac{\gamma_1^2}{4\alpha_1^2}(I2_4+I2_5)\right\}\\&+Q_{i_1}I2_6+Q_{i_1}^2\left\{\frac{\gamma_1}{2\alpha_1}(I2_4+I2_5)-I2_7+\frac{\gamma_1I2_5}{8\alpha_1}\right\}\\&+Q_{i_1}^3\left\{\frac{I2_4}{3}-\frac{I2_5}{3}\right\}+Q_{i_1}^4I2_{14}\\&+\frac{I2_8+I2_9+I2_{10}+I2_{11}+I2_{12}+I2_{13}}{4\alpha_1(32Q_{i_1}L_\mathrm{e}^2\alpha_1^6v_{\mathrm{sat}}^2+16\gamma_1L_\mathrm{e}^2\alpha_1^5v_{\mathrm{sat}}^2)}\\&\frac{\log(\gamma_1+2Q_{i_1}\alpha_1)\{I2_{15}+I2_{16}+I2_{17}\}}{64L_\mathrm{e}^2\alpha_1^6v_{\mathrm{sat}}^2}\\&+\frac{\log(\gamma_1+2Q_{i_1}\alpha_1)\{I2_{18}+I2_{19}+I2_{20}\}}{64L_\mathrm{e}^2\alpha_1^6v_{\mathrm{sat}}^2}\end{aligned} \tag{40}$$

where $\varrho_1=(2A_{11}c_1(1+m_1)+3B_{11}(1+m_1)^2)$, $\varrho_2=2m_1A_{11}+2A_{11}+B_{11}m_1^2+2B_{11}m_1+B_{11}$, $\varrho_3=3A_{11}c_1+6B_{11}m_1+6B_{11}+B_{11}^2m_1^2+2B_{11}^2m_1+B_{11}^2$, $\varrho_4=(2A_{11}c_1m_1+2A_{11}c_1+B_{11}(m_1+1)^2)$ and finally

$$S_{\mathrm{id}}=I1+I2 \tag{41}$$

The induced gate current spectral density following the Klaassen–Prins

IET Circuits Devices Syst., 2016, Vol. 10, Iss. 1, pp. 62–67

equation [17] is

$$S_{ig} = CC_1 \int_{V_s}^{V_d} g_c^2(V) \left(\underbrace{\int g_c(V')QG\mathrm{d}V'}_{PI} \right)^2 \mathrm{d}V \tag{42}$$

where$CC_1 = 4kT\omega^2 W^2/I_d^5 L_e^2$ and $QG = [Q_i(V') - Q_i(V)]$

The inner integral can be written as

$$PI = \int \mu \cdot \mu_{pe} W Q_i \left[1 + \left(\frac{\mu}{v_{sat}} \frac{\mathrm{d}V'}{\mathrm{d}y} \right)^2 \right]^{1/2} QG\mathrm{d}V' \tag{43}$$

which yields

$$PI = \int_{V_s}^{V_d} \mu \cdot \mu_{pe} W Q_i \chi \{ Q_i(V') - Q_i(V) \} \mathrm{d}V' \tag{44}$$

where $\chi = \left[1 + \left(\frac{\mu}{v_{sat}} \frac{(A_{11}Q'_{i_1} + B_{11})}{(2\alpha_1 L Q'_{i_1} + \gamma_1 L)} \right)^2 \right]^{1/2}$

Equation (44) can be written as

$$PI = \int_{V_s}^{V_d} \mu \cdot \mu_{pe} W Q_i \big(\chi Q_i(V') - \chi Q_i(V) \big) \mathrm{d}V' \tag{45}$$

This results in a solution of the form

$$PI = \mu \cdot \mu_{pe} W (N_1 - Q_i N_2) \tag{46}$$

Using this in (42), we obtain

$$S_{ig} = CC_2 \int_{V_s}^{V_d} \left[Q_i^2 + \left(\frac{\mu Q_i^2}{v_{sat}} \frac{\mathrm{d}V}{\mathrm{d}y} \right)^2 \right] (N_1 - Q_i N_2)^2 \mathrm{d}V \tag{47}$$

where $CC_2 = CC_1 \mu \cdot \mu_{pe} W$ and finally we obtain

$$S_{ig} = CC_2 (T_{e_1} + T_{e_2}) \tag{48}$$

where

$$T_{e_1} = \int_{V_s}^{V_d} Q_i^2 (N_1 - Q_i N_2)^2 \mathrm{d}V$$

$$T_{e_2} = \int_{V_s}^{V_d} \left(\frac{\mu Q_i^2}{L v_{sat}} \frac{(A_{11}Q_{i_1} + B_{11})}{(2\alpha_1 Q_{i_1} + \gamma_1)} \right)^2 (N_1 - Q_i N_2)^2 \mathrm{d}V$$

The cross-correlation spectral density is given by [17, 19]

$$S_{igid^*} = -\mathrm{j}CC_3 \int_{V_s}^{V_d} g_o^2(V) \left(\underbrace{\int g_c(V')QG\mathrm{d}V'}_{PI} \right) \mathrm{d}V \tag{49}$$

where $CC_3 = 4kTwW/I_d^3 L_e^2$.

Evaluating the inner integral in the same as in (43) gives

$$S_{igid^*} = -\mathrm{j}CC_4 \int_{V_s}^{V_d} Q_i^2 (N_1 - Q_i N_2)(A_{11}Q_{i_1} + B_{11}) \mathrm{d}Q_{i_1} \tag{50}$$

where $CC_4 = CC_3 [\mu \cdot \mu_{pe} W]^3$.

The final analytical solution for S_{ig} and S_{igid} is too long to include in the manuscript.

2.2 Flicker noise

Flicker noise is generally observed at low frequency and is commonly termed as $1/f$ noise. Generally, the origin of flicker noise is attributed to the following theories:

2.2.1 Carrier number fluctuation theory: According to the theory proposed by McWorther's the origin of flicker noise is due to the tunnelling of charge carriers in traps located in gate dielectric [20]. The fluctuation in charge carriers leads to a fluctuation in surface potential and hence to channel carrier density [20]. Every single trap leads to a Lorentzian noise power spectrum and these Lorentzian spectra add up to give a $1/f$ spectrum.

2.2.2 Mobility fluctuation theory: On the basis of Hooge's theory, the flicker noise is attributed to bulk mobility fluctuations caused by phonon scattering [20]. However, it is observed through experimental results that the origin of flicker noise has a much more complicated dependence on structural parameters and bias condition than suggested by the above two theories. Therefore, a unified theory that incorporates both carrier number fluctuation and mobility fluctuation was proposed [3] to explain flicker noise. Since both the number fluctuation and mobility fluctuation have the same origin and therefore, they are correlated. According to this unified correlated model we have [20]

$$\frac{\delta I_{ds}}{I_{ds}} = -\left[\frac{1}{\Delta N_{inv}} \frac{\delta \Delta N_{inv}}{\delta \Delta N_t} \pm \frac{1}{\mu_{eff}} \frac{\delta \mu_{eff}}{\delta \Delta N_t} \right] \delta \Delta N_t \tag{51}$$

From [20–22], we have

$$\frac{\delta \Delta N_{inv}}{\delta \Delta N_t} = \frac{Q_i}{Q_i + C_{ox} U_T}$$

$$\frac{\delta \mu_{eff}}{\delta \Delta N_t} = -\frac{\alpha \mu_{eff}^2}{W \Delta x}.$$

Following the same evaluation as in [22], we obtain:

$$S_{\Delta I_d}(x, f) = \left(\frac{I_d}{W} \right)^2 \left[\frac{q}{Q_i + C_{ox} U_T} + \alpha \mu \right]^2 N_t \frac{kTW}{\eta f} \tag{52}$$

Here, the expression for α is taken to be the same as in [22]. The drain current spectral density is given by

$$S_{id} = \frac{1}{I_d L_e^2} \int_{V_s}^{V_d} g_o(V) \left[1 + \left(\frac{\mu}{v_{sat}} \frac{\mathrm{d}V}{\mathrm{d}y} \right)^2 \right]^2 S_{\Delta I_d} \mathrm{d}V \tag{53}$$

Evaluating this with (6–8), we get the flicker noise as

$$S_{id} = FC_1 \int_{Q_{i_{1s}}}^{Q_{i_{1d}}} Q_i \left[1 + \left(\frac{\mu}{v_{sat}} \frac{(A_{11}Q_{i_1} + B_{11})}{(2\alpha_1 Q_{i_1} + \gamma_1)} \right)^2 \right] \left[\frac{q}{Q_i + C_{ox} U_T} + \alpha \mu \right]^2 (A_{11}Q_{i_1} + B_{11}) dQ_{i_1} \tag{54}$$

where $FC_1 = I_{ds} N_t kT \mu / L_c^2 \eta f$.

The final analytical solution for flicker noise is also too long to include in the manuscript.

3 Results and discussions

We have validated our model against the two-dimensional TCAD simulation results [11] for devices having gate-oxide thickness asymmetry: $t_{ox_1} = 1$ nm, $t_{ox_2} = 1.5$ nm, $t_{si} = 10$ nm, $L = 35$ nm, $W = 1$ µm. The values of saturation velocity v_{sat} and saturation voltages V_{sat_1}, V_{sat_2} are taken to be the same as in [10]. The values of various other model parameters is taken as $E_f = 6.48 \times 10^{-6}$ V/m, $N_t = 10^{23}$ cm^{-3} eV^{-1}, $\eta = 10^{10}$ m^{-1}, av = 0.22, $m_q = 0.216$.

Fig. 2 shows the thermal noise drain current spectral density for a sweep of gate voltage, V_{gs} from 0 to 2 V predicted from TCAD simulation and proposed model. Fig. 3 shows the thermal noise gate current spectral density for a sweep of drain voltage V_{ds} from 0 to 2 V predicted from TCAD simulation and proposed model. Fig. 4 shows the cross-correlation spectral density for a sweep of frequency from 1 to 20 GHz at $V_{gs} = 1$ V and $V_{ds} = 1$ V for two devices having $L = 35$ and 100 nm predicted from TCAD simulation and the proposed model. It is observed that for all plots the results obtained from TCAD simulation and the proposed model matches accurately. Our model works very well for varied range of bias conditions and operating frequency.

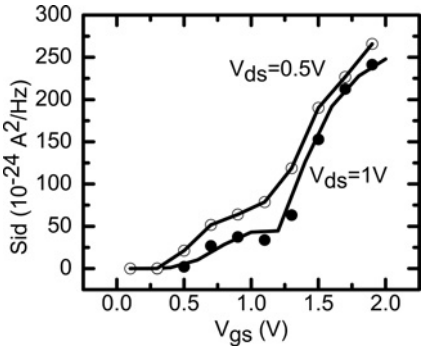

Fig. 2 *Thermal noise drain current spectral density plot with variation in gate voltage for frequency f = 5 GHz predicted from TCAD simulation (symbol) and proposed model (line)*

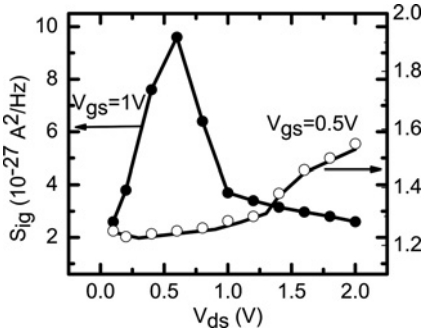

Fig. 3 *Thermal noise gate current spectral density plot with variation in drain voltage at frequency f = 5 GHz predicted from TCAD simulation (symbol) and proposed model (line)*

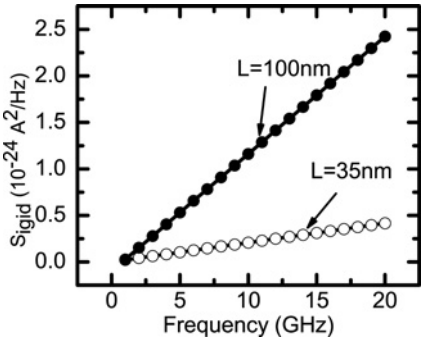

Fig. 4 *Imaginary part of cross-correlation spectral density plot with variation frequency at $V_{gs} = 1$ V and $V_{ds} = 1$ V predicted from TCAD simulation (symbol) and proposed model (line)*

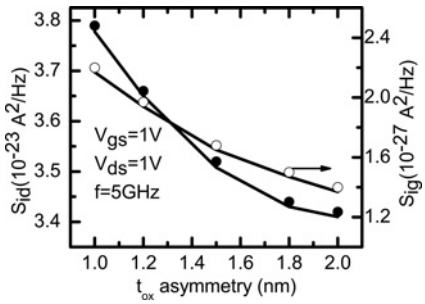

Fig. 5 *Thermal noise drain current spectral density plot with variation in oxide thickness asymmetry at frequency f = 5 GHz, $V_{gs} = 1$ V and $V_{ds} = 1$ V predicted from TCAD simulation (symbol) and proposed model (line)*

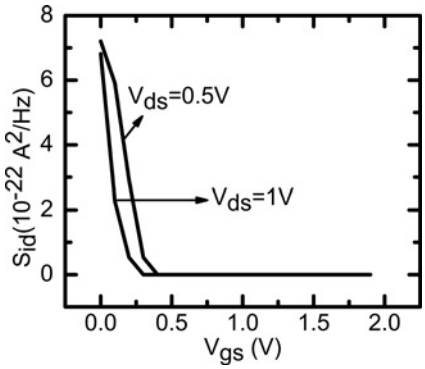

Fig. 6 *Flicker noise drain current spectral density plot with variation in gate voltage at frequency, f = 5 GHz predicted from proposed model*

Fig. 5 shows the impact of asymmetry in oxide thickness on the thermal drain and gate current spectral density. It is observed that with the increase in asymmetry in oxide thickness, the drain and gate current spectral density decreases by 10 and 36%, respectively.

Fig. 6 shows the flicker noise drain current spectral density for a sweep of gate voltage V_{gs} from 0 to 2 V at frequency $f = 5$ GHz predicted from the proposed model. Since, in TCAD there is no model available for simulating flicker noise, we could not match our results. However, it is observed from the plot that the characteristics as well as the values are coming to be in the same range as predicted from the experimental results for FinFETs [23].

Finally, it is worth noting that mathematically the proposed noise model for asymmetric CDG-MOSFET is very simple in nature and can be easily implemented in a circuit simulator.

4 Conclusion

We propose an RF thermal and flicker noise model for CDG-MOSFET based on the linear relationship between surface potentials. The model is adapted to gate-oxide-thickness asymmetry which may prevail in the device due to the process uncertainty. To make the model applicable for short-channel devices we have incorporated the effect of field-dependent mobility in the model. The model is found to be in agreement

IET Circuits Devices Syst., 2016, Vol. 10, Iss. 1, pp. 62–67

with TCAD simulation for varied range of operating conditions and device structures.

5 Acknowledgments

This work was supported by the Department of Science and Technology, Government of India, under Ramanna Fellowship grant number: SR/S3/EECE/0123/2011

6 References

1 Wong, H.S.P: 'Beyond the conventional transistor', *IBM J. Res.Dev.*, 2003, **46**, (2-3)
2 Colinge, J.P.: 'FinFETs and other multi-gate transistors' (Springer-Verlag, 2008)
3 Scholten, A.J., Tiemeijer, L.F., Langevelde, R., *et al.*: 'Noise modeling for RF CMOS circuit simulation', *IEEE Trans. Electron Devices*, 2003, **50**, (3), pp. 618–632
4 Jayaraman, R., Sodini, C.G.: 'A 1/f noise technique to extract the oxide trap density near the conduction band edge', *IEEE Trans. Electron Devices*, 1989, **36**, (9), pp. 1773–1782
5 McWhorter, A.L.: '1/f noise and germanium surface properties' (Semiconductor Surface Physics, University of Pennsylvania Press, Philadelphia, PA, 1957), p. 207
6 Hooge, F.N., Kleinpenning, T.G.M., Vandamme, L.K.J.: 'Experimental studies on 1/f noise'. Reports On Progress in Physics., 1981, 44, pp. 497–532
7 Vandamme, E.P., Vandamme, L.K.J.: 'Critical discussion on unified 1/f noise models for MOSFETs', *IEEE Trans. Electron Devices*, 2000, **47**, (11), pp. 2146–2152
8 Knoblinger, G., Klein, P., Tiebout, M.: 'A new model for thermal channel noise of deep-submicron MOSFETs and its application in RF-CMOS design', *IEEE J. Solid-State Circuits*, 2001, **36**, (5), pp. 831–837
9 Ong, S.N., Chew, K.W.J., Yeo, K.S., *et al.*: 'A new unified model for channel thermal noise of deep sub-micron RFCMOS'. IEEE Int. Symp. on Radio-Frequency Integration Technology, Singapore, 2009, pp. 280–283
10 Sharan, N., Mahapatra, S.: 'A short channel common double gate MOSFET model adapted to gate oxide thickness asymmetry', *IEEE Trans. Electron Devices*, 2014, **61**, (8), pp. 2732–2737
11 'ATLAS, Device simulation framework, Version 5.18.3.R', Users' Manual [online] (Silvaco International, USA, 2012). Available at: www.silvaco.com
12 Sallese, J.M., Krummenacher, F., Pregaldiny, F., *et al.*: 'A design oriented charge-based current model for symmetric DG MOSFET and its correlation with the EKV formalism', *Solid State Electron.*, 2005, **49**, (11), pp. 485–489
13 Dessai, G., Dey, A., Gildenblat, G., *et al.*: 'Symmetric linearization method for double-gate and surrounding-gate MOSFET models', *Solid State Electron.*, 2009, **53**, (11), pp. 548–556
14 Lin, C-H., Dunga, M.V., Niknejad, A.M., *et al.*: 'A compact quantum-mechanical model for double-gate MOSFET'. Solid-State and Integrated Circuits Conf. (ICSICT), Shanghai, 2006, pp. 1272–1274
15 Lime, F., Iniguez, B., Moldovan, O.: 'A quasi-two-dimensional compact drain-current model for undoped symmetric double-gate MOSFETs including short channel effects', *IEEE Trans. Electron Devices*, 2008, **55**, (6), pp. 1441–1448
16 Yamaguchi, K.: 'Field-dependent mobility model for two-dimensional numerical analysis of MOSFETs', *IEEE Trans. Electron Devices*, 1979, **26**, (7), pp. 1068–1074
17 Langevelde, R.V., Paasschens, J.C.J., Scholten, A.J., *et al.*: 'New compact model for induced gate current noise', Int. Electron Devices Meet. *IEDM*, USA, 2003, pp. 36.2.1–36.2.4
18 Jandhyala, S., Kashyap, R., Anghel, C., *et al.*: 'A simple charge model for symmetric double-gate MOSFETs adapted to gate-oxide-thickness asymmetry', *IEEE Trans. Electron Devices*, 2012, **59**, (4), pp. 1002–1007
19 Lazaro, A., Cerdeira, A., Nae, B., *et al.*: 'High-frequency compact analytical noise model for double-gate metal–oxide–semiconductor field-effect transistor', *J. Appl. Phys.*, 2009, **105**, pp. 034510-01–034510-09
20 Hung, K.K., Ko, P.K., Hu, C., *et al.*: 'A unified model for the flicker noise in metal–oxide–semiconductor field-effect transistors', *IEEE Trans. Electron Devices*, 1990, **37**, (3), pp. 654–665
21 Reimbold, G.: 'Modified 1/f trapping noise theory and experiments in MOS transistors biased from weak to strong inversion- influence of interface states', *IEEE Trans. Electron Devices*, 1984, **31**, (9), pp. 1190–1198
22 Li, Z., Ma, J., Ye, Y., *et al.*: 'Compact channel noise models for deep-submicron MOSFETs', *IEEE Trans. Electron Devices*, 2009, **56**, (6), pp. 1300–1308
23 Wei, C., Xiong, Y-Z., Zhou, X.: 'Investigation of low-frequency noise in N-channel FinFETs from weak to strong inversion', *IEEE Trans. Electron Devices*, 2009, **56**, (11), pp. 2800–2810